Available online at www.sciencedirect.com
ScienceDirect
Trans. Nonferrous Met. Soc. China 30(2020) 1491−1499
Transactions of Nonferrous Metals Society of China
www.tnmsc.cn

# Effect of cooling conditions on corrosion resistance of friction stir welded 2219-T62 aluminum alloy thick plate joint

Wei-feng XU[1,2], Jun MA[1,2], Miao WANG[1,2], Hong-jian LU[1,2], Yu-xuan LUO[1,2]

1. State Key Laboratory of Solidification Processing, Northwestern Polytechnical University, Xi'an 710072, China;
2. Shaanxi Key Laboratory of Friction Welding Technologies, Northwestern Polytechnical University, Xi'an 710072, China

Received 23 July 2019; accepted 21 April 2020

**Abstract:** Friction stir welding (FSW) with water cooling and air cooling was used to weld 2219-T62 aluminum alloy joints with a thickness of 20 mm. The effect of cooling conditions on the corrosion resistance of joints in 3.5% NaCl solution was investigated using the open circuit potential (OCP), the potentiodynamic polarization, and the corrosion morphology after immersing for different time. And the precipitates distribution was characterized by scanning electron microscopy (SEM) and transmission electron microscopy (TEM). The results reveal that the weld nugget zone (WNZ) owning positive potential, lower corrosion current density and fine and uniform precipitates, is much more difficult to corrode than the heat affected zone (HAZ) and the base metal (BM). Compared with air-cooled joint, the water-cooled joint has better corrosion resistance. In addition, the results of microstructure observation show that the potential, distribution and size of second phase particles determine the corrosion resistance of FSW AA2219 alloy joints in chlorine-contained solution.

**Key words:** friction stir welding; aluminum alloy; air cooling; water cooling; corrosion resistance; second phase particles

## 1 Introduction

Aluminum and its alloys are characterized by low price, low density, excellent cryogenic properties, ease of manufacture and relatively high strength [1]. High-strength 2xxx series aluminum−copper alloy 2219 is widely applied in aerospace and other engineering fields due to a combination of good mechanical properties and high resistance to stress corrosion [2]. Because of the existence of intermetallic compounds formed through the alloying and heat treatment, the material obtains the above desirable properties [3]. However, the formation of intermetallic compounds increased the structural heterogeneity, which results in the high sensibility to form localized corrosion, like pitting or intergranular corrosion, mainly in chlorine-contained environments [4,5].

Welding is an important means to reduce the manufacturing cost of complex structures. It is easy to form melting and solidification defects if the traditional fusion welding method is adopted for joining aluminum alloy. And these defects will result in a significant reduction of the service performance, including corrosion resistance [6]. Friction stir welding (FSW), as a solid state welding technology, brings a revolutionary leap to the welding of aluminum alloys [6−9]. However, unlike welding aluminum alloy sheets, lots of studies have

**Foundation item:** Project (51405392) supported by the National Natural Science Foundation of China; Project (2019T120954) supported by the China Postdoctoral Science Foundation; Project (3102019MS0404) supported by Fundamental Research Funds for the Central Universities, China; Project (2018BSHQYXMZZ31) supported by the Postdoctoral Science Foundation of Shaanxi Province, China
**Corresponding author:** Wei-feng XU; Tel/Fax: +86-29-88492624; E-mail: xwf1982@nwpu.edu.cn
DOI: 10.1016/S1003-6326(20)65313-4

been carried out to prove the presence of large temperature gradients and uneven mechanical plastic deformation in different regions along the thickness direction of plate in FSW thick plate joints process [7−12]. As a result, an uneven distribution of second phase particle is formed. In the classical corrosion studies, grain size and distribution of second phase particles are the primary factors affecting the corrosion resistance of materials [6]. Previous findings on the FSW of aluminum alloys indicated that the atmospheric corrosion behavior of welds is of technological importance when the workpieces are exposed to a NaCl-induced atmospheric environment, for instance, in aerospace applications [13]. Therefore, it is necessary to investigate the corrosion resistance in different regions along the thickness direction of FSW thick plate joint of high-strength aluminum alloy.

Cooling condition affects the metallurgical characteristics and precipitation behaviors of FSW joints [14,15]. The previous research [14] has confirmed that by adopting water cooling during FSW process, a more refined microstructure with the fine dispersed particles was obtained and both of strength and ductility were enhanced in 2219 aluminum alloy joints. WANG et al [16] have conducted a study on the corrosion behavior of 4 mm-thick 7055 aluminum alloy joints welded by underwater FSW, and the results indicated that the corrosion potential of underwater joint was more positive and had lower corrosion density compared with the base metal (BM) and traditional joint. In other words, underwater joint possessed better corrosion resistance and lower corrosion rate. Recently, SINHMAR and DWIVEDI [15] have researched the influence of water cooling on the corrosion resistance of FSW 6 mm-thick AA2014 alloy joint, and found that the corrosion resistance was enhanced due to the reduction in the width of heat affected zone (HAZ) and the formation of discontinued and small-size precipitates.

Present studies of FSW joint by water cooling or underwater are just focused on the effect of water cooling on enhancing the corrosion resistance of thin-plate FSW joints, and are seldom related to thick plates. Meanwhile, it is unclear what changes have occurred in the corrosion resistance of the FSW thick plate joints under different cooling conditions. So, this study is mainly focused on the microstructure evolution and corrosion behavior in different regions along the thickness direction of 20 mm-thick 2219 aluminum alloy FSW joints with air cooling and water cooling.

## 2 Experimental

A commercial AA2219-T62 alloy was selected with a length of 300 mm, a width of 150 mm and a thickness of 20 mm. The FSW tool has a shoulder of 34 mm in diameter and a threaded (left-handed screw) cone-shaped pin of 13.5 mm in root diameter and 9.3 mm in tip diameter, and rotated clockwise. Two cooling conditions (air cooling and water cooling) were used during FSW. The air cooling (A1 condition) was achieved by cooling in room temperature atmosphere and the water cooling (W1 condition) was achieved by spraying water to the weld tool and top surface of the weld. All joints were welded under the same FSW parameters with a rotational rate of 300 r/min and a welding speed of 80 mm/min. Meanwhile, a tilt angle of 2.8º was adopted. The macrographs of the cross section of defect-free FSW joints with air cooling and water cooling are shown in Fig. 1.

Transmission electron microscope (TEM FEI 20) was used to observe the distribution of the precipitates in the welded joints with water cooling.

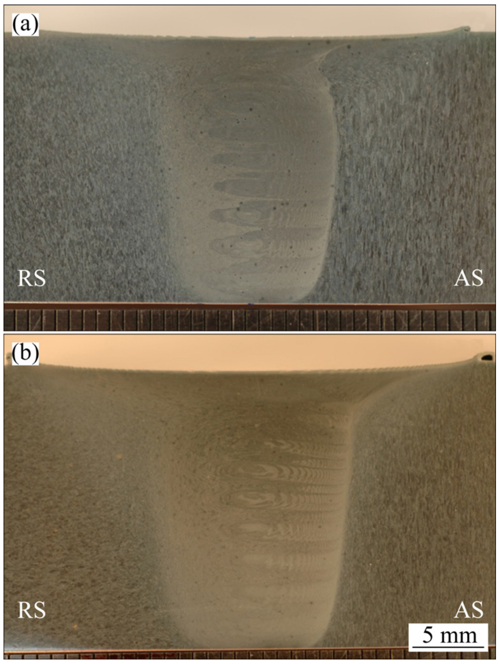


**Fig. 1** Macrographs of FSW 2219 aluminum alloy joints on cross section with air cooling (a) and water cooling (b)

An electrical-discharge machine was used to cut thin foils for TEM observation from corresponding locations in the weld. The thin foils for TEM were then polished by jet electro-polishing employing a solution of 70% methanol and 30% nitric acid at 243 K (−30 °C) and 19 V.

All electrochemical measurements were performed on the specimens. These specimens were mechanically ground with progressive grades of abrasive papers to 7000# and finally polished with 1 μm diamond paste on velvet cloth to mirror surface, washed with distilled water and dried with air blower. All solutions used in experiment were 3.5% NaCl solution prepared with analytical grade reagents and ultrapure water (18.2 MΩ) prepared from Millipore Milli-Q, and were not de-aerated in the experiments. A three-electrode flat cell setup, composed of working electrode, a platinum mesh as counter electrode and a standard calomel electrode (SCE) as reference electrode, was used for all the electrochemical measurements. The sheets were cut from three zones (top, middle and bottom) along the thickness of the plate in 2219-T62 aluminum alloy, the weld nugget zone (WNZ) and the heat-affected zone (HAZ), possessing a bare surface of 0.2 $cm^2$, as working electrode. In order to keep data stable, the open circuit potential (OCP) was recorded from 1 h after the sample was immersed in the 3.5% NaCl solution and maintained for 0.5 h. Then, the potentiodynamic polarization was performed at the scan rate of 1 mV/s. The surfaces were polarized between −500 and 1000 mV relative to the OCP. The electrolyte temperature was maintained at room temperature and the volume of electrolyte was 200 mL. All the experiments were conducted under the computer control.

Firstly, markers were made at the appropriate regions on the top surface, and the top, middle and bottom of weld nugget zone (WNZ-TS, WNZ-T, WNZ-M and WNZ-B, respectively), the thermo-mechanical affected zone (TMAZ), the HAZ and the base material (BM). Then, the images were taken in the zones around the markers via SEM. Finally, the samples were taken out of the SEM chamber and immerged in the 3.5% NaCl solution at room temperature. After desired immersing time (1, 4, 10, 24 and 48 h, respectively), the samples were dried and put into the SEM chamber again. The corrosion morphology was recorded around the markers. This process was repeated after every desired immersing time was reached to provide the evolution images of the corrosion.

## 3 Results and discussion

### 3.1 Open circuit potential

Figure 2 shows the open circuit potential (OCP) versus time curves obtained with FSW joints under different cooling conditions immersed in 3.5% NaCl solution. The incipient OCP increases markedly during the first several minutes of immersion, which indicates that spontaneous passivation occurs on all the electrode surfaces, except for HAZ. The OCP of samples shifting to more anodic direction is often related to the formation of protective passive film on the alloy surface [17,18]. And then, the OCP slowly shifts negatively with small fluctuations until it tends to the level. This is mainly because the chloride ions start attacking the surface of material in contact with the sodium chloride solution. Meanwhile, the reformation of a thin air-formed alumina film is also a dominant factor for the drop [19]. The formation and dissolution of passive film in dynamic competitive equilibrium are the main causes of fluctuations. However, it is difficult to observe the spontaneous passivation in HAZ from the open circuit potential curves. Both of HAZs present a smaller fluctuation compared with other zones. This also confirms that the formation and the dissolution of the passivation film in HAZ show a dynamic competitive equilibrium when the sample contacts with 3.5% NaCl solution.

It can be observed that the OCP of the joints with water cooling changes to more positive

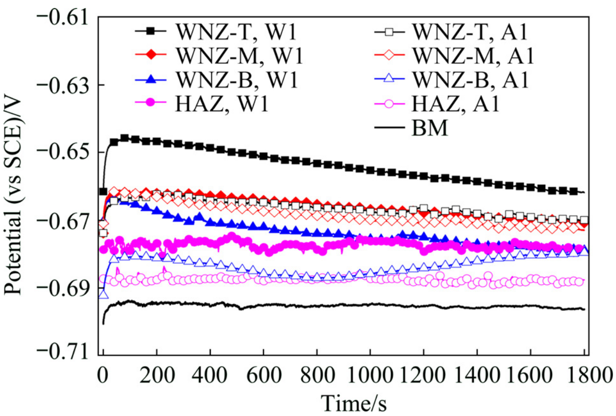


**Fig. 2** Open circuit potentials of different zones in air (A1) and water-cooled (W1) joints and BM in 3.5% NaCl solution

potential than that of the joints with air cooling. This might be caused by the fine second phase particles and the lack of precipitate free zone (PFZ) formed due to the larger cooling rate and the shorter time at high temperature with water cooling [14]. Meanwhile, it is possible that anodic grain boundary precipitates appear in the weld zones with air cooling. The curves distinctly indicate that, at different positions of WNZ, the WNZ-T presents a relatively higher open circuit potential than that of WNZ-M and WNZ-B. The WNZ-T has weaker electrochemical activity and higher corrosion resistance. It is also clearly revealed in Fig. 2 that different positions of WNZ have more positive potential than HAZ and BM. In other words, in comparison with HAZ and BM, the electrochemical activity of WNZ decreases and corrosion resistance is improved after FSW process. Moreover, the value of OCP presents a slight reduction for the WNZ of A1 and W1 joints, which shows that the corrosion resistance slightly decreases with the increase of immersion time. For example, the initial OCP of BM is −0.701 V, then it sharply increases to a maximum of −0.695 V and remains around this value within 1800 s before the end of immersion test. The initial and maximum OCP values of the top, middle and bottom of WNZ with water cooling are given in Table 1. The BM and HAZ show negative potential, which means that they own the larger electrochemical activity. Compared with the BM and A1 joint, both the WNZ and HAZ of W1 joint have positive potential, which demonstrates that it possesses higher corrosion resistance. Thus, the corrosion resistance of FSW joint with water cooling can be improved compared with air cooling. The corrosion testing result reveals that the corrosion resistance of water-cooled 2014 Al alloy joint is better than that of air-cooled joint [15].

**Table 1** Initial and maximum OCP of different zones of FSW joints and BM in 3.5% NaCl solution

| Sample | Location | Initial OCP (vs SCE)/V | Maximum OCP (vs SCE)/V |
|---|---|---|---|
| BM | − | −0.701 | −0.695 |
| W1 | WNZ-T | −0.662 | −0.645 |
| | WNZ-M | −0.674 | −0.661 |
| | WNZ-B | −0.692 | −0.680 |
| | HAZ | −0.682 | −0.674 |
| Al | WNZ-T | −0.671 | −0.660 |
| | WNZ-M | −0.671 | −0.662 |
| | WNZ-B | −0.692 | −0.681 |
| | HAZ | −0.690 | −0.684 |

### 3.2 Potentiodynamic polarization

The potentiodynamic polarization curves obtained from the joints immerged in 3.5% NaCl solution for WNZ and HAZ along the thickness direction are shown in Fig. 3. The curves obtained from different positions of the WNZ and HAZ with water cooling, compared with the BM and air-cooled joints, present much more positive corrosion potential ($\varphi_{corr}$) and lower corrosion current density ($J_{corr}$). In other words, the corrosion tendency becomes weaker after FSW and the water cooling makes it weaker further. It can be observed from Fig. 3 that the corresponding pitting potential ($\varphi_{pit}$) of WNZ with water cooling is more positive, indicating that the water cooling is adverse to pitting corrosion. In another word, the lower susceptibility of material to pitting corrosion for WNZ with water cooling is obtained. It can be

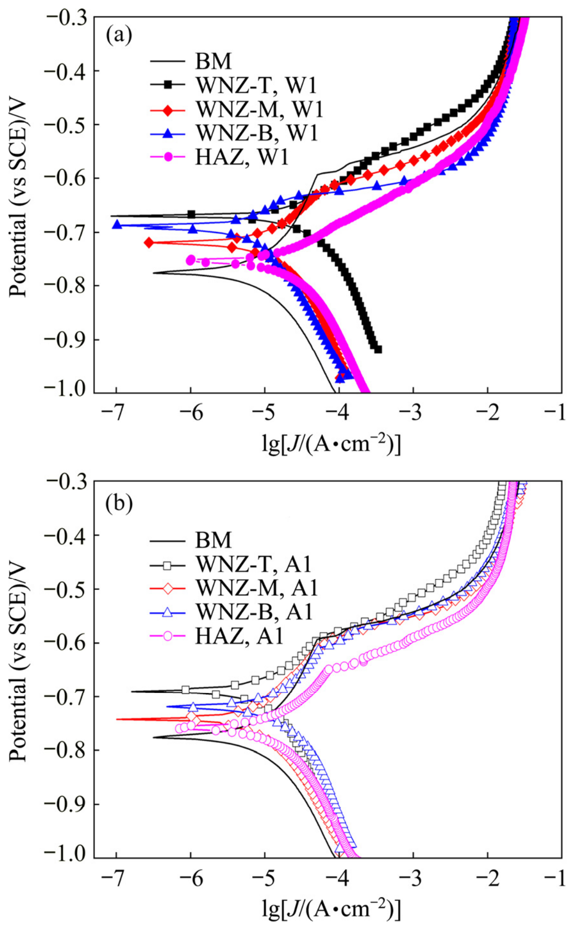


**Fig. 3** Potentiodynamic polarization curves of WNZ and HAZ of joints with water cooling (a) and air cooling (b)

concluded that the pitting potential has the same change in corrosion resistance as the corrosion potential.

### 3.3 In-situ observation of corrosion attack

For the selected 2219 aluminum alloy, two kinds of second phase particles can be found in the BM. The results of SEM/EDS analysis of two different typical second phase particles (gray and bright particles) are shown in Fig. 4. From the EDS line scan of six elements (Al, Cu, Mg, Mn, Fe and Si) shown in Fig. 4, it is easy to identify two typical particles: Al−Cu−Mg−Mn−Fe−Si phase (named as Fe-containing phase-gray particle) and $Al_2Cu$ ($\theta$ phase-bright particle).

The corrosion morphologies of different zones of FSW joints immerged in 3.5% NaCl solution maintained for different immersion time are shown in Fig. 5.

The microstructure of the BM is composed of large elongated and pie-shaped grains (~150 μm in the thickness direction and ~500 μm in the longitudinal direction) with reticular second phase particles on initial grain boundaries, as shown in Fig. 5. EDS analysis reveals that the initial grain boundary phase is mainly $Al_2Cu$ bright particles combined with gray particles containing aluminum, copper, manganese, magnesium and silicon, as shown in Fig. 3. The distribution and size of second phase particles in different weld zones, which have experienced various thermal cycle and plastic deformation, present significant difference. The second phase particles in WNZ-TS are obviously coarser than those in other zones, such as WNZ-T and WNZ-M. However, the larger intermetallics gather in WNZ-B caused by the lack of large plastic deformation. The deformed grains in the TMAZ are bent and elongated in an upward flow pattern because of the shearing action of the welding tool. The particles distribute along the direction of deformed grains. The size distributions of two types of particles in the HAZ do not change significantly compared with the BM and particles have partly dissolved. This is only attributed to the thermal cycle.

For three types of microstructures, the potential of the bright $\theta$ phase ($Al_2Cu$) is most noble in comparison to that of the gray particles and Al matrix, and the order of potential is as follows: $\theta$ phase > gray particles > Al matrix [17,20]. The noble precipitate acts as the cathode and the Al matrix acts as the anode when the joints are in contact with the corrosion solution. No obvious corrosion pits are observed on the surface of samples after being immersed in NaCl solution for 1 h. The pitting corrosion occurs in every zone when the immersion time reaches 4 h. The incipient galvanic couple of pitting corrosion is established between the fine dispersed $\theta$ phase particles and their adjacent aluminum matrix. The aluminum

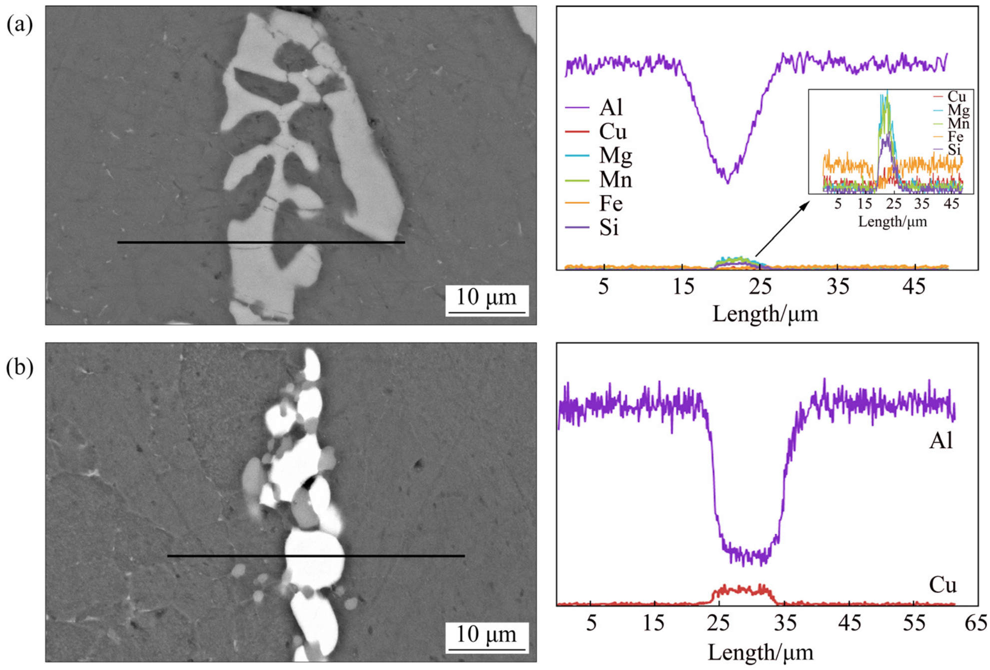


**Fig. 4** EDS line scans of second phase particles in BM: (a) Al−Cu−Mg−Mn−Fe−Si phase; (b) $Al_2Cu$ phase

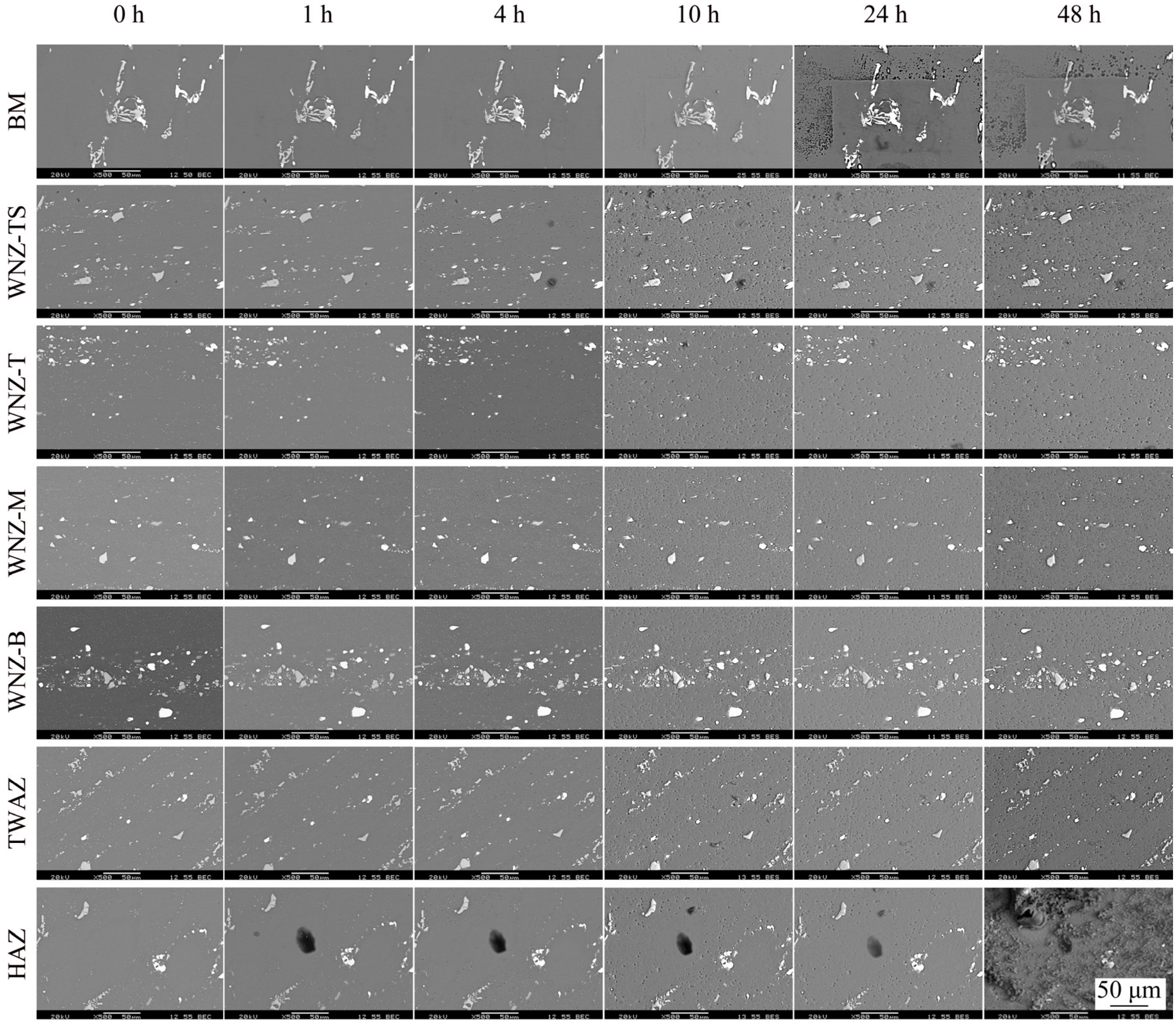


**Fig. 5** Corrosion morphologies in BM and different zones of FSW joint with water cooling after different immersion time

matrix as the anode takes priority in dissolving because it has the lower self-corrosion potential compared with the adjacent $\theta$ phase particles and gray particles. As the immersion time increases, the pitting corrosion becomes more and more serious, which means that the Al matrix around the particles is dissolved continuously during the initial stage. Moreover, it can be seen from Fig. 5 that the Al matrix (anode) around the bright particle (cathode) gets more preferentially dissolved than the gray particles around the bright particle, which is attributed to the larger potential difference between the bright particle and the Al matrix. After 10 h of immersion, lots of pits are scattered around the second phase particles in the WNZ and TMAZ. However, part of the second phase particles precipitates along the grain boundary and the aluminum matrix with the larger particles around it is dissolved to form pits in the HAZ. When the immersion time increases to 24 h, the density and size of pits increase. The BM shows a larger number of pits than the weld zones. The WNZ presents a slight pitting corrosion, especially for the WNZ-T and WNZ-M. When the immersion time reaches 48 h, lots of corrosion products cover the surface of HAZ and the pits expand to BM.

According to these results, it can be concluded that the corrosive occurs obviously in zones adjacent to the intermetallic particles. Meanwhile, a intenser localized corrosion is observed in both the BM and HAZ, and the pitting is deeper and larger, which is consistent with above result that the BM and HAZ have much more negative open circuit potential and pitting potential, as shown in Fig. 3. The reduction in the size of intermetallic particles in WNZ is attributed to the decrease of the intensity of the galvanic cell founded between the intermetallic particles and the Al matrix, leading to a less corrosive attack in the WNZ. This is exactly consistent with the previous researches reported by JIANG et al [21] and VACCHI et al [22]. The forming tendency of galvanic cell between Al matrix and intermetallic particles with finer sizes decreases, so the sensitivity to pitting corrosion in WNZ reduces. Meanwhile, second phase particles in the BM and HAZ gather together to form larger cluster-like particles, which is not conducive to the formation of a uniform and dense passivation film on the surface. Invasive $Cl^{-}$ anions are easily wedged into the passivation film from the weak areas to form small hole, which becomes a corrosion active point. These corrosion cores continue to grow until the formation of pitting corrosion. This repeats to form an autocatalytic process, and many corrosion pits gather to achieve local dissolved corrosion. Therefore, the BM and HAZ have poorer corrosion resistance.

### 3.4 Effect of precipitates distribution on corrosion resistance

The TEM images of the precipitates in the BM and different positions of WNZ, TMAZ and HAZ are shown in Fig. 6. It is clear that some changes in the morphology of the precipitates in weld has occurred compared with that of the BM. The quantity of the precipitates in the weld decreases due to the dissolution of the precipitates resulted from experiencing thermal-mechanical effect of the FSW tool, especially for the WNZ.

The rod-like and needle-shaped precipitates are frequently seen in the matrix of AA2219 zones but do not present in the WNZ-T and WNZ-M, which shows that dissolution, re-precipitation and redistribution of intermetallics have occurred. Except for the recrystallization of the plastically deformed grains, the temperature (sometimes higher than 530 °C) during FSW is in the solution thermal-treatment range for these alloys. The temperature is adequate for dissolution and re-precipitation of most precipitates in the BM. Along the thickness direction, the WNZ-T and WNZ-M present small spherical precipitates compared to the WNZ-B. The WNZ-B, which is not completely spheroidized due to undergoing lower frictional thermal cycle and smaller mechanical stirring during FSW process, shows only some spherical and rod-like precipitates, as shown in Fig. 6(d).

Compared with the BM (Fig. 6(a)), the amount of the precipitates presents an obvious decrease and

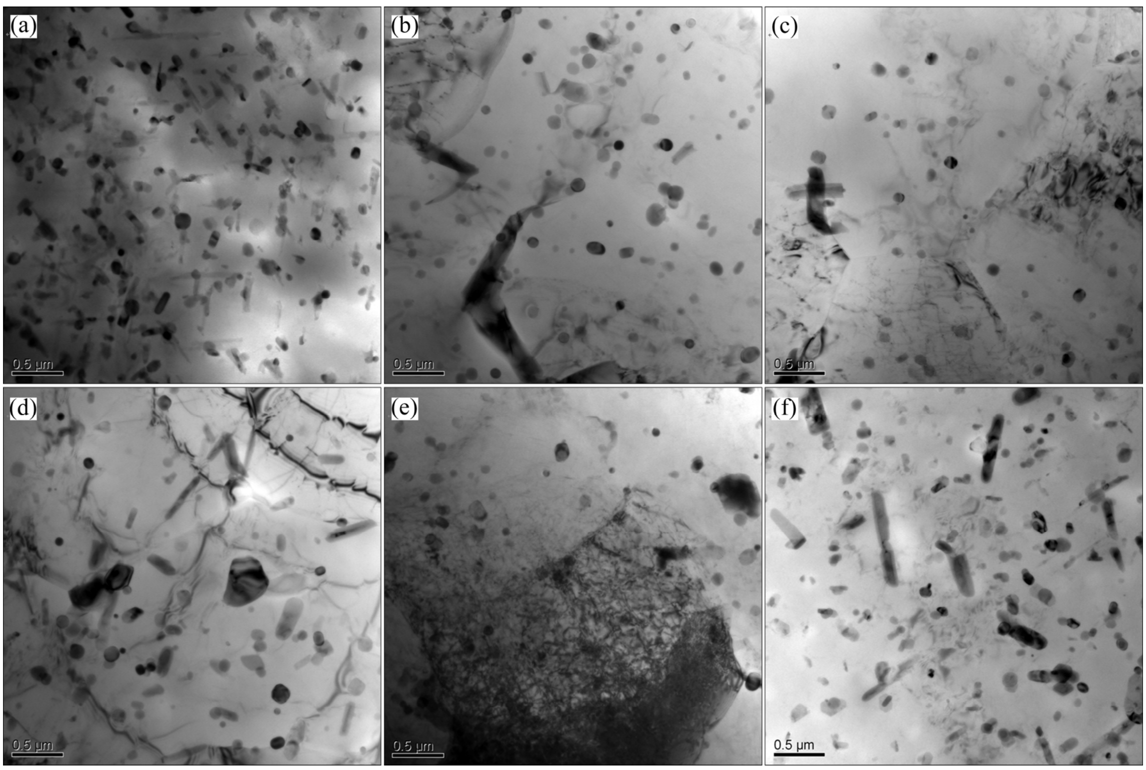


**Fig. 6** TEM micrographs of precipitates in BM (a), top (b), middle (c) and bottom (d) of WNZ, TMAZ (e) and HAZ (f)

the shape is changed from the rod-like and the needle-shaped into small spherical in the WNZ, as shown in Figs. 6(b, c). This contributes to reducing the potential difference between the high potential of precipitates and the low potential of Al matrix, making the reaction of local galvanic cell difficult to occur and improving the corrosion resistance. Moreover, the rod-like and needle-shaped precipitates are relatively easy to absorb the chloride ions compared with the small spherical precipitates, confirming that the WNZ has higher potential and lower corrosion current density during the electrochemical measurement process.

## 4 Conclusions

(1) The WNZ of FSW joints presents much more positive open circuit potential, corrosion potential, pitting potential and lower corrosion current density than HAZ and BM of AA2219 alloy.

(2) The significantly improved corrosion resistance is obtained in water-cooled joint due to lower electrical activity, higher potential and lower current density compared with air-cooled joint.

(3) Pitting corrosion occurs and aggravates with the increase of immersion time in chloride solution. Some evenly distributed small pits, lots of corrosion products and pits expansion can be seen in the WNZ, HAZ and BM when the immersion time reaches 48 h, respectively.

(4) The amount of the precipitates in the weld containing the small spherical precipitates decreases compared with BM, especially for WNZ. The WNZ-T and WNZ-M present basically complete spheroidization. But a small amount of spheroidization occurs in HAZ having larger rod-like precipitates. This reduces the corrosion resistance of HAZ and BM.

## References

[1] LI Shuai, DONG Hong-gang, LI Peng, CHEN Su. Effect of repetitious non-isothermal heat treatment on corrosion behavior of Al−Zn−Mg alloy [J]. Corrosion Science, 2018, 131: 278−289.

[2] WANG Hui-min, YI You-ping, HUANG Shi-quan. Influence of pre-deformation and subsequent ageing on the hardening behavior and microstructure of 2219 aluminum alloy forgings [J]. Journal of Alloys and Compounds, 2016, 685: 941−948.

[3] COLLAZO A, NÓVOA X R, PÉREZ C. The role of $Mg^{2+}$ ions in the corrosion behaviour of AA2024-T3 aluminium alloys immersed in chloride-containing environments [J]. Electrochimica Acta, 2014, 124: 17−26.

[4] LARIGNON C, ALEXIS J, ANDRIEU E, BLANC C, ODEMER G, SALABURA J C. Corrosion damages induced by cyclic exposure of 2024 aluminium alloy in chloride-containing environments [J]. Journal of the Electrochemical Society, 2011, 158: 284−295.

[5] ZHU Dan-qing, van OOIJ W J. Corrosion protection of AA 2024-T3 by bis-[3-(triethoxysilyl)propyl] tetrasulfide in neutral sodium chloride solution. Part 1: Corrosion of AA 2024-T3 [J]. Corrosion Science, 2003, 45: 2163−2175.

[6] SINHMAR S, DWIVEDI D K. A study on corrosion behavior of friction stir welded and tungsten inert gas welded AA2014 aluminium alloy [J]. Corrosion Science, 2018, 133: 25−35.

[7] XU Wei-feng, LUO Yu-xuan, FU Ming-wang. Micro-structure evolution in the conventional single side and bobbin tool friction stir welding of thick rolled 7085-T7452 aluminum alloy [J]. Materials Characterization, 2018, 138: 48−55.

[8] XU Wei-feng, WU Xu-kun, MA Jun, LU Hong-jian, LUO Yu-xuan. Abnormal fracture of 7085 high strength aluminum alloy thick plate joint via friction stir welding [J]. Journal of Materials Research and Technology, 2019, 8: 6029−6040.

[9] MARTINEZ N, KUMAR N, MISHRA R S, DOHERTY K J. Microstructural variation due to heat gradient of a thick friction stir welded aluminum 7449 alloy [J]. Journal of Alloys and Compounds, 2017, 713: 51−63.

[10] GUO Ning, FU Yun-long, WANG Yu-zhong, MENG Qiang, ZHU Yu-xiao. Microstructure and mechanical properties in friction stir welded 5A06 aluminum alloy thick plate [J]. Materials and Design, 2017, 113: 273−283.

[11] ABDULSTAAR M A, AL-FADHALAH K J, WAGNER L. Microstructural variation through weld thickness and mechanical properties of peened friction stir welded 6061 aluminum alloy joints [J]. Materials Characterization, 2017, 126: 64−73.

[12] IMAM M, SUN Y F, FUJII H, MA N S, TSUTSUMI S, MURAKAWA H. Microstructural characteristics and mechanical properties of friction stir welded thick 5083 aluminum alloy [J]. Metallurgical and Materials Transactions A, 2017, 48: 208−229.

[13] ESMAILY M, MORTAZAVI N, OSIKOWICZ W, HINDSEFELT H, SVENSSON J E, HALVARSSON M, THOMPSON G E, JOHANSSON L G. Corrosion behaviour of friction stir-welded AA6005-T6 using a bobbin tool [J]. Corrosion Science, 2016, 111: 98−109.

[14] XU Wei-feng, LIU Jin-he, CHEN Dao-lun, LUAN Guo-hong, YAO Jun-shan. Improvements of strength and ductility in aluminum alloy joints via rapid cooling during friction stir welding [J]. Materials Science and Engineering A, 2012, 548: 89−98.

[15] SINHMAR S, DWIVEDI D K. Enhancement of mechanical properties and corrosion resistance of friction stir welded joint of AA2014 using water cooling [J]. Materials Science and Engineering A, 2017, 684: 413−422.

[16] WANG Qing-zhao, ZHAO Yong, YAN Keng, LU Sheng. Corrosion behavior of spray formed 7055 aluminum alloy

joint welded by underwater friction stir welding [J]. Materials and Design, 2015, 68: 97−103.
[17] XU Wei-feng, LIU Jin-he, ZHU Hong-qiang. Pitting corrosion of friction stir welded aluminum alloy thick plate in alkaline chloride solution [J]. Electrochimica Acta, 2010, 55: 2918−2923.
[18] EMREGÜL K C, AKSÜT A A. The behavior of aluminum in alkaline media [J]. Corrosion Science, 2000, 42: 2051−2067.
[19] GARCIA-GARCIA F J, SKELDON P, THOMPSON G E, SMITH G C. The effect of nickel on alloy microstructure and electrochemical behaviour of AA1050 aluminium alloy in acid and alkaline solutions [J]. Electrochimica Acta, 2012, 75: 229−238.
[20] XU Wei-feng, ZHANG Wei, WU Xiao-li. Corrosion behavior of top and bottom surfaces for single-side and double-side friction stir welded 7085-T7651 aluminum alloy thick plate joints [J]. Metallurgical and Materials Transactions A, 2017, 48: 1078−1091.
[21] JIANG J H, MA A B, LU F M, SAITO N, WATAZU A, SONG D, ZHANG P, NISHIDA Y. Improving corrosion resistance of Al−11mass%Si alloy through a large number of ECAP passes [J]. Materials and Corrosion, 2011, 62: 848−852.
[22] VACCHI G S, PLAINE A H, SILVA R, SORDIA V L, SUHUDDIN U F H, ALCÂNTARA N G, KURIA S E, ROVERE C A D. Effect of friction spot welding (FSpW) on the surface corrosion behavior of overlapping AA6181/Ti−6Al−4V joints [J]. Materials and Design, 2017, 131: 127−134.

# 冷却条件对 2219-T62 铝合金厚板搅拌摩擦焊接头耐蚀性的影响

徐韦锋[1,2]，马 骏[1,2]，王 苗[1,2]，卢鸿键[1,2]，罗宇轩[1,2]

1. 西北工业大学 凝固技术国家重点实验室，西安 710072；
2. 西北工业大学 陕西省摩擦焊接工程技术重点实验室，西安 710072

**摘 要**：通过开路电位(OCP)、动电位极化曲线、扫描电子显微镜(SEM)和透射电子显微镜(TEM)研究水冷和空冷对 20 mm 厚 2219-T62 铝合金搅拌摩擦焊(FSW)接头在 3.5% NaCl 溶液中耐蚀性的影响。结果表明，与 2219 铝合金母材和 FSW 焊缝热影响区相比，具有较高电位、较低腐蚀电流密度和细小均匀沉淀强化相的 2219 铝合金 FSW 焊缝焊核区，在 3.5% NaCl 溶液中具有较好的耐蚀性。与空冷接头相比，水冷 FSW 接头的耐蚀性明显提高。通过显微组织形貌分析可知，2219 铝合金 FSW 接头在含氯离子腐蚀溶液中的耐蚀性取决于电位的高低和第二相粒子尺寸和分布。

**关键词**：搅拌摩擦焊；铝合金；空冷；水冷；耐蚀性；第二相粒子

**(Edited by Bing YANG)**